Fatigue & Fracture of Engineering Materials & Structures

WILEY

FFEMS Fatigue & Fracture of Engineering Materials & Structures

ORIGINAL ARTICLE OPEN ACCESS

Effect of Matrix Properties on Quasi-Static and Fatigue Properties of Thermosetting Polyurethane and Its GFRP Composites

Martin Demleitner[1] | Daniel Raps[2] | Sarah Mäker[2] | Qi Chen[3] | Alexander Brückner[1] | Holger Ruckdäschel[1]

[1]Department of Polymer Engineering, University of Bayreuth, Bayreuth, Germany | [2]Covestro AG, Leverkusen, Germany | [3]Covestro Netherlands B.V., Urmonderbaan 22, 6167 RD, Geleen, the Netherlands

Correspondence: Holger Ruckdäschel (holger.ruckdaeschel@uni-bayreuth.de)

Received: 20 January 2025 | **Revised:** 16 January 2026 | **Accepted:** 7 February 2026

Keywords: cross-link density | polyurethane resin | rotor blade | SN curve

ABSTRACT

In this study, the influence of resin cross-link density on thermomechanical properties and fatigue behavior of polyurethane resins and glass fiber-reinforced polyurethane (PUR-GFRP) composites was investigated. This material is a candidate for renewable energy applications like rotor blades in wind turbines. The thermomechanical behavior and morphologies of three different PUR resin systems were analyzed using dynamic mechanical analysis (DMA) and atomic force microscopy (AFM). Results show that the system with low cross-link density exhibits earlier crack initiation but higher strains before failure, indicating initially a more brittle behavior but greater polymer chain reorientation capacity. This phenomenon was correlated to the different phase morphology and the hybrid nature of the investigated PUR resins. Residual strength analysis showed minimum influence on tensile strength and a slight modulus decrease after extensive creep tests. This highlights the importance of fiber–matrix interaction on the composite fatigue failure. The static mechanical properties of the composites and SN fatigue tests allowed assessing the fatigue performance and lifetime analysis under specific loading conditions. Highly cross-linked systems show a significantly longer lifetime compared to the medium cross-linked system. In conclusion, the study highlights the importance of understanding resin cross-link density's impact on fatigue behavior in GFRP composites for better material and part design.

1 | Introduction

The increasing global electricity demand and shift towards renewable energies, projected to rise from 22,000 TWh in 2020 to 30,000 TWh in 2030, is partially met with the installation of solar and wind energy plants. Wind turbines are considered one of the most environmentally friendly sources presently available, generating up to 40 times more energy over their lifetime in comparison to their manufacturing process [1, 2]. To maximize energy production and cost competitiveness, rotor blades are becoming larger, with the current turbine V236–15.0 MW featuring the world's longest blade at 115 m.

Rotor blades for wind turbines are usually made of resin reinforced with glass or carbon fibers by vacuum infusion (e.g., shear web and shell) or pultrusion technology (e.g., spar caps). In modern rotor blade designs, some key mechanical properties are high stiffness, tensile and compressive strength, and good fatigue resistance under dynamic loading. The resin matrix plays a critical role in transferring loads through the fiber network and must possess desired properties such as stiffness (elastic modulus), yield stress, ultimate strength, and fracture toughness. Other factors such as thermal properties, processability, cost, availability, and minimum hazardous substances are also of great importance. While the fibers

Summary

- Effect of cross-link density on fatigue behavior of polyurethane resins and its composites.
- Low cross-link density systems exhibit earlier crack initiation, indicating brittle behavior.
- Residual strength analysis showed that fiber–matrix interaction plays a role in fatigue failure.
- Highly cross-linked systems demonstrate longer lifetimes under specific loading conditions.

dominate mechanical properties of the composites like elastic modulus and strength, the matrix properties strongly influence fatigue failure. Matrix cracks, debonding, and delamination may eventually occur during operation. Currently, epoxy (91% market share) and polyester resins (9% market share) are commonly used, but they have specific drawbacks in terms of processing and blade performance [3]. Epoxy resins have limited potential for increase in mechanical performance and reducing production cycle time and minimizing curing temperatures.

As promising alternative, polyurethane resin (PUR), offers cost-efficiency and low viscosity for faster impregnation of longer and thicker blades, as well as low to moderate curing temperatures in combination with low reaction enthalpy for increased productivity rates. However, polyurethanes are inherently sensitive to moisture, generating challenges when manufacturing blade shells with balsa wood as core material. Balsa wood typically contains 6–12 wt % of water, necessitating sufficient drying before considering the use of PUR [4–6]. The trend of using PVC and PET foams instead of balsa wood is advantageous for the application of PURs. Even though glass fibers still contain moisture on their surface, thorough drying is necessary to produce parts without residual porosity [7]. Drying can be done very efficiently with both vacuum and a small purge of inert gas as nitrogen, although drying requires time, this additional step is outweighed by the other benefits of PUR resins [8]. In addition to processing advantages (e.g., low viscosity, low exothermy, and fast curing), PUR-based resins often offer attractive mechanical properties for composite parts subjected to fatigue, particularly high (fracture) toughness.

Although PURs usually show good intrinsic fracture toughness, certain improvement is in general possible by modifying the network structure or by adding fillers or toughening. This generally leads to better (fatigue) crack behavior in both neat resin and composites.

It is noteworthy that the matrix toughness is especially important for biaxial composites (fiber in ±45° direction), where high shear loading on the matrix and fiber–matrix interface takes place. Although carbon fibers possess high modulus in fiber direction, the modulus transverse to the fiber direction is quite low due to the graphitic layer structure. Here, glass fibers have a higher modulus and therefore at constant loading direction the matrix in GFRPs has to withstand higher strain compared to CFRPs [9]. Therefore mechanical behavior tends to be "matrix-dominated" for ±45°, especially with glass fiber reinforcement.

In this case, a tougher matrix needs only to withstand a certain strain until the fiber reinforcement restrains the elongation development of the matrix. This was clearly shown by Altstädt et al. [10]. Thus, only a certain resin toughness can be transferred into the composite as a large increase in resin toughness has not necessarily been found to give a proportionate increase in composite toughness.

Only few publications deal with the characterization of the neat resin system and the transfer to the fatigue behavior of its composite. Figure 1 gives an overview of available literature. Further information about the individual resin system, modification, reinforcement, and loading conditions can be found in the table in Supporting Information. Since fracture toughness measurements were carried out only rarely, the strain at break was used as a rough indicator for the resistance to fatal failure [11], Gassan et al. showed that impact-modified epoxy resin in GFRP had less stiffness reduction during fatigue trials at a given strain compared to the brittle, nonmodified EP matrix and could withstand 14× more cycles [12]. The impact-modified composites, however, showed a more nonlinear SN-curve (in log–log-scale) and "sudden death" behavior in contrast to linear behavior for the brittle matrix. In another study by Manjunatha et al., carboxyl-terminated poly(butadiene-coacrylonitrile) (CTBN) and silica nanoparticles suppressed matrix cracking in an epoxy-GFRP system and reduced crack growth rate leading to six to 10 times longer lifetimes under tensile fatigue loading [13]. Certain toughness of the resins generally helps in delaying the microcracking and thus enhancing the fatigue life of the composites [14].

Generally, there is a lack of consensus in published studies regarding the impact of matrix modification on fatigue life. Some reports indicate an improvement in fatigue life by matrix modification, while others suggest the opposite effect; see Figure 1 [11, 15, 16]. Besides matrix properties and modification via additives, additional variables such as fiber layup, fiber volume content, and loading conditions pose challenges when attempting to determine the underlying causes for the observed variations in fatigue life.

As a notable trend, the impact of toughening diminishes as the applied loads increase, primarily because at these elevated stress levels, the toughening agent's ability to deter plastic deformation and cracking appears to be less effective [17–19]. There is only one publication by Joneja et al. where the resin itself was modified by mixing a brittle and a tough polyester resin. Here, deteriorated fatigue properties with higher fracture strain are visible [15].

In general, the presence of a matrix with excessive toughness can have detrimental effects on the fatigue behavior of composites under unidirectional loading, as demonstrated in the cases of PEEK/CF (polyetheretherketone/carbon fiber) and Epoxy/CF (epoxy/carbon fiber) composites. Despite possessing higher toughness, PEEK/CF composites exhibited steeper slopes in fatigue behavior, primarily attributed to a weaker interface between the fibers and the matrix, resulting in significant debonding [20, 21].

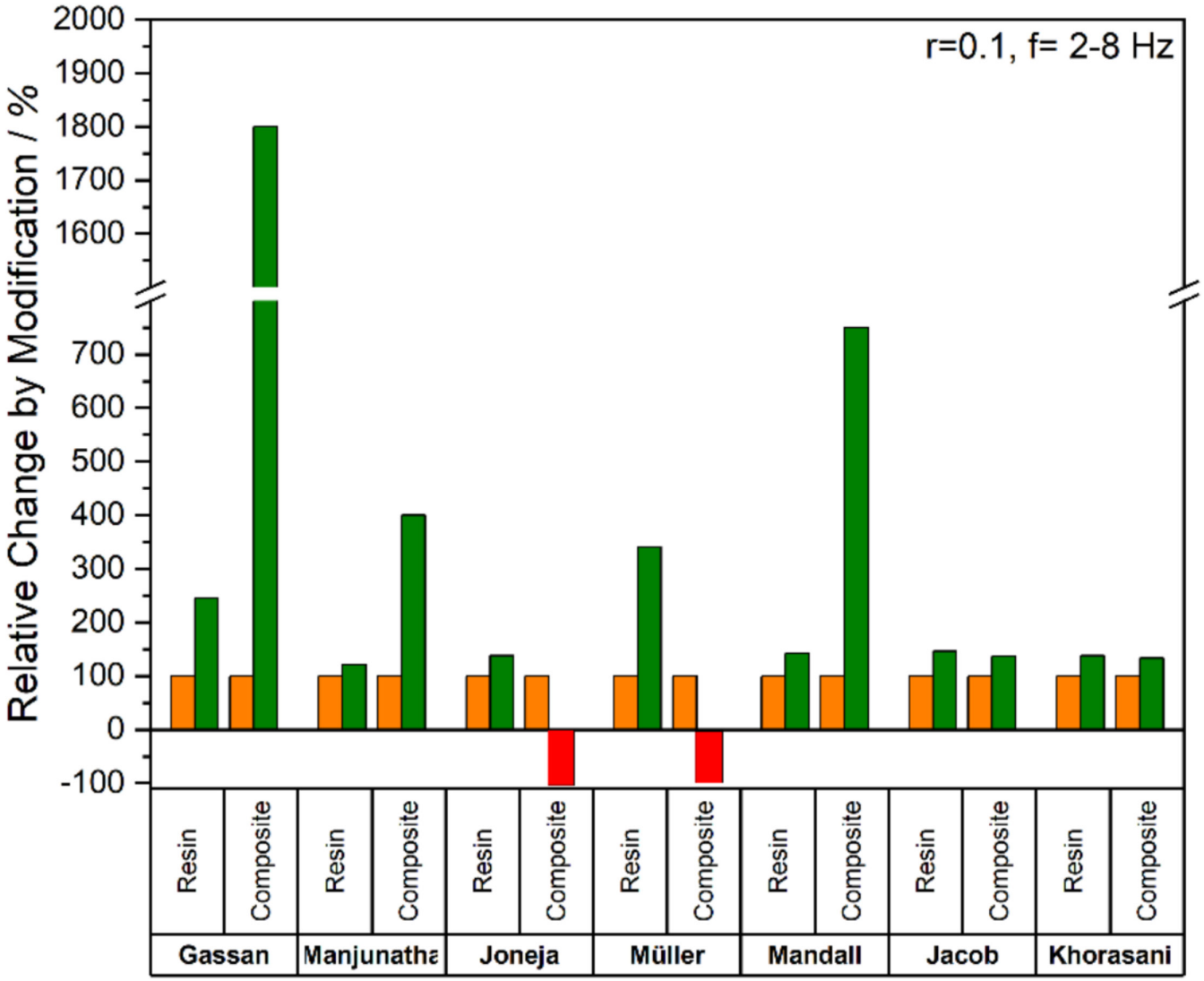

FIGURE 1 | Literature overview of resin modification and impact on the composite fatigue properties, in green improvement in fatigue properties was shown, in red deterioration in fatigue properties with resin modification/toughener were determined (details about resin modification, laminate properties, and testing conditions can be found in Supporting Information). [Colour figure can be viewed at wileyonlinelibrary.com]

Based on these findings and previous observations, it is evident that an optimum balance between stiffness and strength with toughness exists for polymeric matrices for composites to ensure overall favorable fatigue resistance. A sufficiently high stiffness and strength reduce the deformation around the fibers and keep the material intact also at stress peaks, and a high toughness prohibits cracks from possible defects or fatigue from fast growth. Unfortunately, stiffness and strength increase with a higher cross-link density (CLD), while toughness decreases due to hindered chain mobility and thus reduced ductility. Furthermore, it is essential to incorporate composite constituents that suppress progressive debonding and longitudinal matrix cracking, thereby enhancing fatigue resistance. Apart from the interaction between the fibers and the resin, the formation or nucleation of cracks within the resin phase can also impact fatigue behavior and the overall lifetime of the composite material. It appears that higher strength levels contribute to the reduction of crack nucleation, as observed in creep experiments conducted on epoxy resins [22].

When considering the literature on failure mechanisms, there needs to be a balance between slow crack growth and slow crack nucleation/generation. In highly cross-linked materials, one would expect slow crack nucleation but faster crack growth, whereas the opposite holds true for low(er) cross-linked systems. However, without conducting fatigue testing on different cross-link densities, it is challenging to determine which factor dominates in each system. In this context, the strength and toughness of a material are governed by the resin network and, consequently, the cross-link density [23–25].

Figure 2 provides a comprehensive overview of the relationship between resin cross-link density and the glass transition temperature (T_g) for various types of thermoset resins. T_g is chosen as a thermomechanical property since it is easily accessible and measurable. Moreover, many applications require a minimum glass transition temperature, e.g., rotor blades need to exceed a T_g of 65°C [50]. Figure 2 demonstrates that higher cross-link density generally leads to higher achievable T_g values. Polyurethanes are particularly advantageous as they achieve

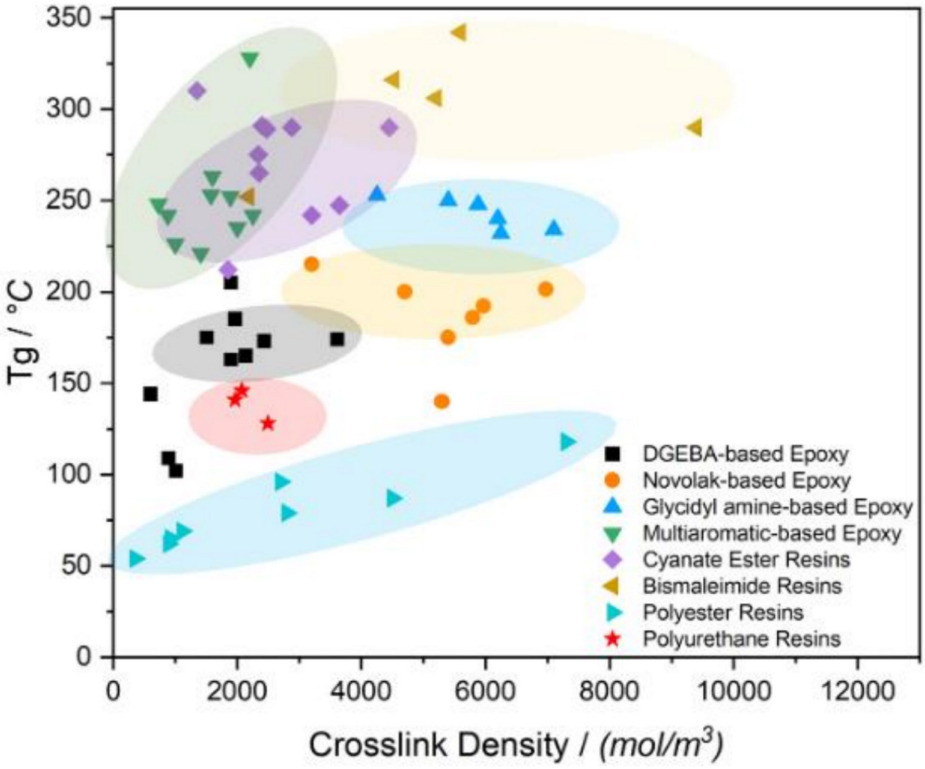

FIGURE 2 | Overview of cross-link density values and corresponding glass transition temperature for different thermoset resin systems polyester resins [26–30], bismaleimide resins [31, 32], cyanate ester resins ([33–38], multiaromatic-based epoxy [39–41], glycidyl amine-based epoxy [42, 43], novolac-based epoxy [44, 45], DGEBA-based epoxy [42, 43, 46–49], and polyurethane resin (this work)). [Colour figure can be viewed at wileyonlinelibrary.com]

a sufficiently high T_g even at relatively low cross-link density values. This results in a less constrained network, enabling the material to exhibit improved toughness compared to polyester or epoxy resin systems.

Interestingly, the scientific literature on the influence of the resin on the fatigue properties of the composite is scarce as mentioned earlier and this especially holds true for thermosetting PURs. Among the few research studies conducted in this area, Kempf et al. investigated the compression fatigue of impacted polyurethane-glass fiber-reinforced polymer (PUR-GFRP) in comparison to epoxy-GFRP, revealing superior fatigue performance in PUR composites [51]. Gloggnitzer et al. studied the influence of manufacturing parameters (curing temperature and curing pressure) on the flexural fatigue performance of PUR-GFRP [52]. Huelsbusch et al. explored damage progression using hysteresis, microcomputed tomography (μ-CT), and temperature measurements during load-increase fatigue tests of PUR-GFRP [53, 54]. A recent review summarizes current knowledge on PUR-based composites, focusing on the influence of environmental factors on their mechanical properties [55].

Existing literature acknowledges the importance of matrix resin strength and toughness in shaping the fatigue behavior of composites through crack management and fiber interactions. However, there is a distinct lack of research exploring the influence of matrix properties, or more specifically, resin cross-linking density on fatigue properties in composites overall. From the perspective of material development, the objective is to create composites with prolonged lifetimes by identifying the optimal cross-linking density. Hence, it is crucial to determine whether cross-linking density can still be further optimized in future resin formulations. Consequently, the aim of the present study is to assess crack initiation and growth in neat PUR resins with different cross-linking densities, as well as the tensile fatigue performance of their corresponding GFRP composites.

2 | Experimental

2.1 | Materials and Processing

To investigate the effect of cross-link density on (thermo)mechanical and fatigue properties, three different PURs based on polymeric isocyanate, polyether polyols, and an OH-functional reactive thinner were studied. The cross-link density was controlled by polyol functionality, molecular weight, and composition. In this frame, a decreasing molecular weight of the polyether polyol as well as an increased content of the reactive thinner result in a higher PUR-cross-link density at constant NCO/OH-ratio ("index") and vice versa.

Formulation A, serving as the reference with medium cross-link density (CLD), consisted of polyol mixture A (OH-Value = 356 mg KOH/g, viscosity at 25°C = 38 mPas) and a polymeric isocyanate (30.8% NCO, viscosity at 25°C = 190 mPas). The mixing ratio of polyol to isocyanate was 100:88, resulting in an index of 102.

Formulation B with high CLD consists of polyol mixture B (OH-Value = 448 mg KOH/g, viscosity at 25°C = 24 mPas) and the

abovementioned polymeric isocyanate, mixing ratio polyol/isocyanate 100:111, index 102.

Formulation C with low CLD consists of polyol mixture C (OH-Value = 259 mg KOH/g, viscosity at 25°C = 96 mPas) and the abovementioned polymeric isocyanate, mixing ratio polyol/isocyanate 100:64, index 102.

From these formulations, both neat resin plates (NRP) and composite test plates were produced according to the following procedures.

2.1.1 | Preparation of Neat Resin Plates

The resin components were mixed and degassed at about 1 mbar for 20 min and subsequently poured into a glass mold with silicone rubber lining. The plates were cured in an oven with a defined temperature profile. Beforehand, the glass mold was dried for 1 h at 40°C, and the resin poured in at 40°C. All plates were heated from 40°C to 80°C with a heating rate of 0.5 K/min and finally cured isothermally at 80°C for 3 h. After curing, the plates were left in the oven to cool down to RT and demolded the day after. The manufactured NRP had a thickness of approximately 4 mm.

The degree of cure (DOC) of all NRP was determined via residual enthalpy from DSC measurements (0°C–220°C with 10 K/min, N_2) in relation to the reaction enthalpy of the components (10 K/min, 0°C–220°C) with reference to DIN EN ISO DIN EN ISO 11357-1 and −5. The DoC ranged from 91% for NRPB, 97% of NRP A to 99% of NRP C.

2.1.2 | Preparation of Glass Fiber Composites

The layup and materials are shown in Figure 3 from bottom to top: electrical aluminum heating plate, mold with release agent, flow mesh, perforated foil, peel ply, two layers of biax glass (Saertex X-E 1210, areal weight of 1210 g/m^2), peel ply, VAP membrane CS/E, textile fleece as spacer, two spiral hoses for inlet and outlet of resin, vacuum foil attached with tacky tape, temperature sensors on top of layup, and on mold surface, isolation blanket to cover layup.

The mold and fiber layup were dried for 2 h at 35°C under vacuum (~1 mbar). A sufficient amount of polyol/isocyanate mixture (respective mixing ratio, index 102) was stirred and degassed for 10 min at about 1 mbar before starting the vacuum infusion from a disposable container. When the layup was filled, the curing cycle (heat to 80°C with 0.5 K/min and keep at 80°C for 3 h) was initiated while covering the layup with an isolation blanket. The setup was left under vacuum at open resin inlet while heating up to allow for the compensation of shrinkage. After cooling to room temperature overnight, the cured laminate was demolded.

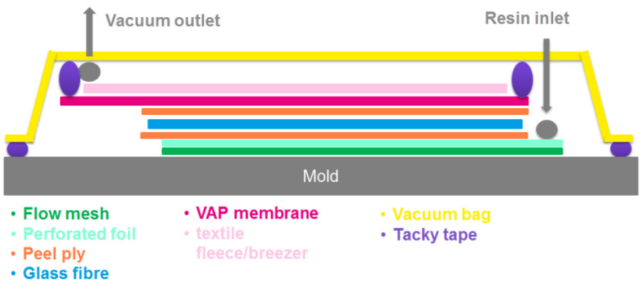

FIGURE 3 | Layup for composite production. [Colour figure can be viewed at wileyonlinelibrary.com]

2.2 | Characterization

If not stated differently, all tests were performed at 23°C and 50% relative humidity.

2.2.1 | Dynamic Mechanical Analysis (DMA)

DMA measurements were performed to determine the thermomechanical behavior of the resin formulations; storage and loss modulus, T_g, and cross-link density were obtained. DMA measurements can also provide an insight into the phase morphology based on the shift in T_g, broadening of tan(δ) peaks or shoulders depending on miscibility as well as morphology. DMAs were carried out at a heating rate of 3°C/min in torsional mode at an elastic deformation of 0.1% and a frequency of 1 Hz (Rheometrics Scientific ARES RDA III, Germany). The specimens have a rectangular shape with 50 × 10 × 2 mm^3 according to standard ISO 6721-7. The glass transition temperature was evaluated at the maximum of the loss factor, tan(δ). The determined storage modulus in the rubbery plateau region can be considered inversely proportional to the chain length (Mc) between cross-links [56, 57]. In order to calculate the cross-link density v_c, Equation (1) was used:

$$v_c = \frac{G'}{RT} = \frac{E'}{3RT}, \tag{1}$$

where G′ is the storage modulus in the rubber elastic plateau (i.e., obtained 50°C above T_g), R is the gas constant (=8.314 J/mol·K), E′ is the Young's modulus at the respective temperature. Here, the cross-link density is the amount of elastically effective network chains per unit volume.

2.2.2 | Neat Resin Tensile Tests

Tensile properties of the neat resin were determined using a Zwick Universal Testing Machine (Zwick Roell Group, Ulm, Germany) equipped with a 20 kN load cell. Dog-bone shaped 1B-specimen with 150 × 20 × 4 mm^3 sample geometry were fabricated using a CNC milling machine (Mutronic Präzisionsgerätebau GmbH & Co. KG, Rieden, Germany). The tests were carried out according to DIN ISO 527-1 at a crosshead speed of 5 mm/min. Minimum of five valid measurements were performed per material.

2.2.3 | Fatigue Crack Measurements da/dN

Fatigue crack propagation (FCP) measurements were conducted to gain insights into the long-term crack resistance and microdamage tolerance, specifically focusing on initial crack

nucleation, crack growth, and overall ductility of the resin systems. The fatigue crack growth behavior can be categorized into three distinct regimes. In the first phase, the crack initiation is characterized by the threshold value (ΔK_{th}). The second phase corresponds to stable crack growth propagation, commonly known as the Paris–Erdogan regime, which follows a power law behavior represented by the Equation (2):

$$\frac{da}{dn} = C\,\Delta K^m \tag{2}$$

where a is the crack length, C the growth rate at 1 MPam$^{0.5}$ and m the slope of the cure in the second phase. Subsequently, the third phase is characterized by critical or unstable crack growth, described by ΔK_{cf}.

FCP tests were performed with a computer-controlled servo-hydraulic test machine (Hydropuls MHF, Carl Schenck AG, Darmstadt, Germany) based on ISO15850/ASTM E647. Compact-tension (CT) specimens were used for the FCP testing. A sharp crack is initiated by loading the mounted specimen with a low sinusoidal load. At least three specimens were tested for reproducibility. A detailed overview about the method and calculations is given by Kothmann et al. [58, 59].

2.2.4 | Neat Resin Creep Test

Tensile creep properties were tested on a Zwick Kappa 50-SS creep testing machine (Zwick Roell Group, Ulm, Germany) equipped with a 10-kN load cell and an optical macrodisplacement transducer according to ISO 899-1 using 1B-specimens from ISO-standard 527-1. The stress levels were 50%, 60%, and 70% of the individual ultimate tensile strength σ_{UTS} at room temperature. Testing time was up to 1000 h if no fatal creep rupture had occurred previously. All measurements were carried out at least twice.

Furthermore, to determine the residual strength after creep loading, additional creep tests were performed at a stress level of 60% UTS and terminated once 50% of the quasi-static elongation at break was reached. Subsequently, quasi-static tensile tests were conducted within 24 h to determine the residual strength. The aim was to gain a better understanding of the potential impact of long-term average strain and macroscopic damage evolution during (cyclic) fatigue measurements of the composites.

2.2.5 | Composite Tensile Test

Tensile properties of the biaxial composite were determined using a Zwick Universal Testing Machine (Zwick Roell Group, Ulm, Germany) equipped with a 20-kN load cell. Specimen geometry was $250 \times 25 \times 2\,mm^3$, and specimens were preprepared with GFRP caps. Tests were carried out according to DIN ISO 527-4. A minimum of five valid measurements were performed.

2.2.6 | Composite Tensile Fatigue Tests

During fatigue testing, known also as SN test, material samples undergo repeated loading cycles to gather information regarding the material's endurance limit and to predict the lifetime. The selection of various load levels is based on the individual ultimate static tensile strength, using the pearl string method as outlined in DIN 50100. This method was used for a range of load cycles, in this case ranging from 10^4 to 10^7 cycles. The servo-hydraulic test machine IST IPL50K (Carl Schenk AG Darmstadt, Germany) with IST 8800/Software (Dynmat by BASF AG, Ludwigshafen) at a constant stress ratio of $R = 0.1$ was used. A frequency of 8 Hz was set based on premeasurements where the surface temperature was monitored via an infrared sensor. A maximum frequency of 8 Hz for higher loads was set to ensure that the maximum temperature due to self-heating of the composite was well below 35°C prior fracture to avoid any temperature-induced fracture and fatigue mechanism. The load was set from 30% to 60% of the ultimate composite tensile strength. All edges of the specimens were polished to minimize surface effects and to ensure that cracking initiation within the bulk.

2.2.7 | Atomic Force Microscopy

The morphology of the neat resin was studied by AFM; cross-section of the dog-bone shaped specimen was prepared using a Leica EM TXP (Leica Microsystems, Wetzlar, Germany). A diamond blade rotating at 20000 rpm was used to remove the excess part of the sample, followed by polishing using diamond lapping foil with 2-μm grid size at 2500 rpm, until an optically smooth cross-section surface was obtained. The sample was then mounted onto a vertical sample holder. An AFM image of the cross-section surface was obtained under ambient conditions in tapping mode using a NanoScope V multimode atomic force microscope (Bruker Nano Surfaces, Santa Barbara, CA, USA) equipped with a silicon cantilever having a resonance frequency of 300–400 kHz (Type: TESP-V2, Bruker Nano surfaces, Santa Barbara, CA, USA).

2.2.8 | Scanning Electron Microscopy (SEM)

To evaluate the mode of fracture, the fractured surfaces of the da/dN specimens were observed by Zeiss Leo 1530 SEM (Carl Zeiss AG, Oberkochen, Germany) at an accelerating voltage of 3 kV. The specimens were sputter-coated with gold prior to SEM observations.

3 | Results and Discussion

3.1 | Neat Resin Characterization

3.1.1 | Thermomechanical Profile and Morphology

The loss factors tan(δ) and the storage moduli of the three resins are plotted in Figure 4.

The glass transition temperatures (T_g) based on tan(δ) were determined to be 128°C for the medium cross-linked (CLD) system, 141°C for the high cross-linked system, and 146°C for the low cross-linked system. The reference system exhibited a single peak, while the high and low cross-linked systems showed a bimodal curve, indicating the presence of a second phase. The

bimodal peak and the presence of a second phase, as confirmed by atomic force microscopy (AFM) measurements, can be attributed to the low cross-linked system, which exhibited a significant shoulder starting around 50°C.

The cross-link density of the resin systems plays a critical role in determining their stiffness, toughness, and the properties of the final composite material. The cross-link density was calculated using Equation (1) based on DMA for the three resin systems. The results showed that the alternative resin systems had a lower cross-link density, approximately 20% lower (see Table 1). However, due to the bimodal peak, phase separation tendency, and the continuous decrease in storage modulus observed in the low cross-linked system, these values can only be considered as rough estimates. Additionally, the cross-link density was calculated based on the formulation characteristics such as functionality and molecular weight and compared with the cross-link density obtained from DMA measurements. The difference between the experimental value and theoretically calculated value of CLD is attributed partially due to the dynamic nature of urethane bonds at elevated temperatures and the two-phase morphology. The individual curing kinetics and single or interpenetrating network formations and resulting phase morphology makes it more challenging to obtain valid cross-link density values as shown in literature [60, 61].

In order to elucidate this phase separation, AFM was carried out on the cross sections of the cured neat resins to visualize the morphology of the three samples. The obtained AFM phase images are shown in Figure 5.

As can be seen in the images, the morphology of all three resins is rather different. In the case of medium-CLD resin, a homogeneous phase contrast is observed, with domains of lower phase contrast present sporadically within the materials. In contrast, both low- and high-CLD resins show phase-separated morphologies, while the way of separation is not the same. In the low-CLD resin, the high phase contrast materials form domains of ~40 nm with clear boundaries and are connected via materials with low phase contrast. On the other hand, the high phase contrast materials in high-CLD resin form a continuous matrix, while the low phase contrast materials are embedded as domains of 20 to 40 nm. In the context of the hybrid nature of the polyurethane system applied with soft and hard phases, the high phase contrast materials are believed to be components with high T_g. This continuous high T_g phase in the high-CLD resin is responsible for the second T_g plateau as observed in the DMA curve. In contrast, the enclosed high T_g phase bordered by small amounts of low T_g phase in the low-CLD resin explains the larger separation between the two glass transition temperatures in the tan(δ) plot.

Furthermore, heat deflection temperature (HDT) and tensile properties were determined, following the same trend as the properties obtained by DMA. The respective values are listed in Table 2.

Based on the tensile properties, the medium- and high-CLD systems exhibit similar moduli of around 3.5 GPa, whereas the low-CLD system has a significantly lower modulus of 1.7 GPa. In terms

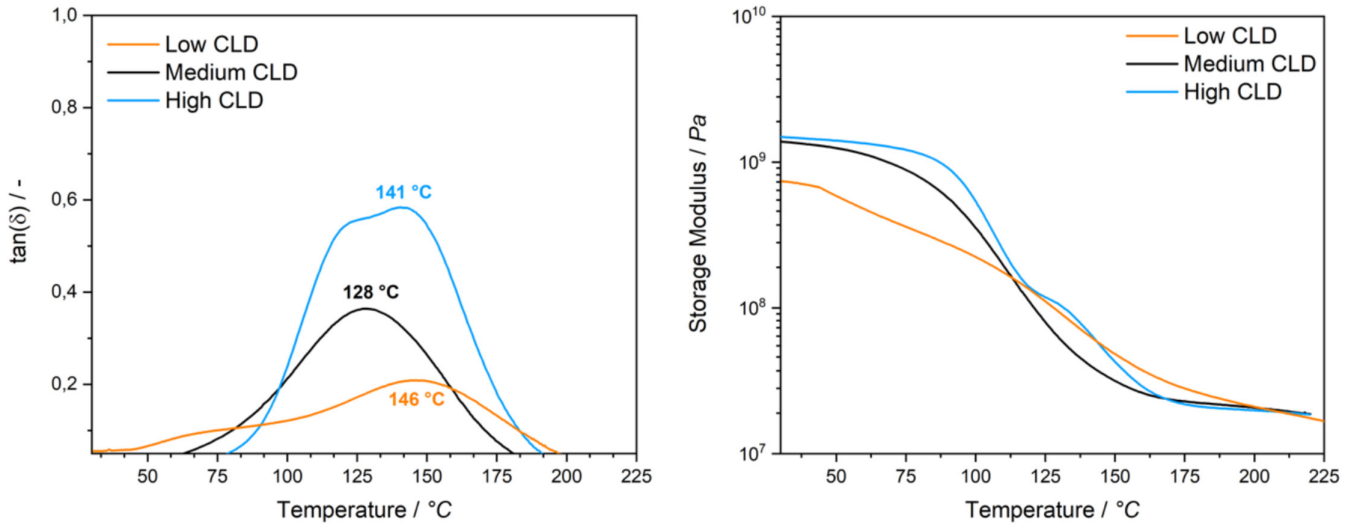

FIGURE 4 | Loss factor and storage modulus of the three different PUR resin systems. [Colour figure can be viewed at wileyonlinelibrary.com]

TABLE 1 | Thermomechanical properties of the three resin systems.

Resin system	Density g/cm³	T_g tan (δ)°C	Storage modulus (RT) Pa	Rubber modulus at T_g + 50 K Pa	Cross-link density mol/m³	Theoretically calculated cross-link density mol/m³
Medium CLD	1.20	128	1.3E9	2.25E7	2495.3	4220
High CLD	1.22	141	1.5E9	2.02E7	1964.3	4590
Low CLD	1.17	146*	7.4E8	2.16E7	2072.7	3770

*broad peak.

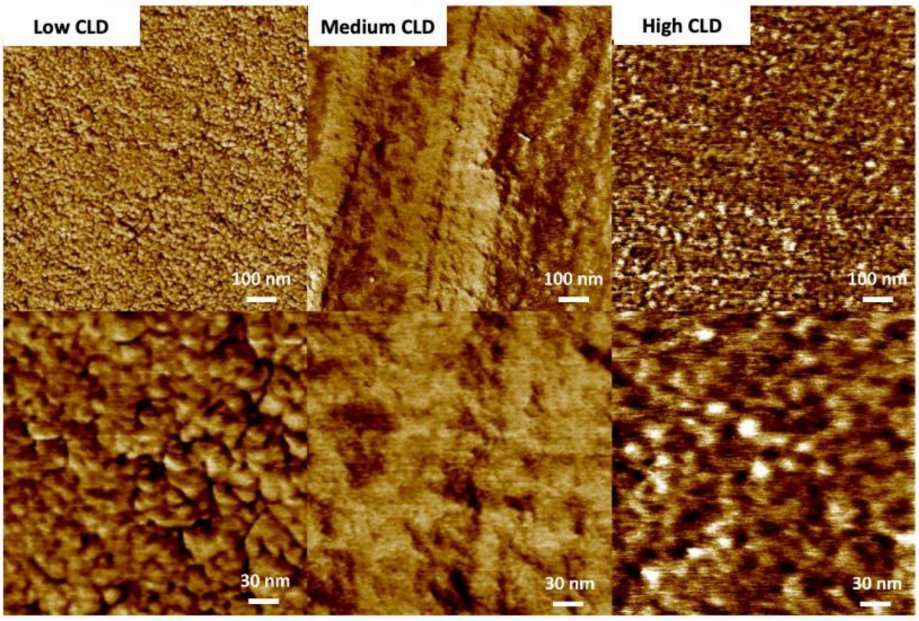

FIGURE 5 | AFM phase images of low-CLD (left), medium-CLD (middle), and high-CLD (right) samples with an image area of $1 \times 1\,\mu m^2$ (top row) and $300 \times 300\,nm^2$ (bottom row); the Z scale is from −5° to 5°. [Colour figure can be viewed at wileyonlinelibrary.com]

TABLE 2 | Heat deflection temperatures (HDT) and tensile properties of the neat resin systems.

Resin system	HDT/°C	Tensile modulus/GPa	Tensile strength/MPa	Elongation at break/%
Low-CLD	71	1.68 ± 0.03	44.8 ± 1	9.3 ± 2.7
Medium CLD	88	3.59 ± 0.17	83.4 ± 1	5.1 ± 0.3
High CLD	91	3.55 ± 0.17	101 ± 0.1	5.4 ± 0.9

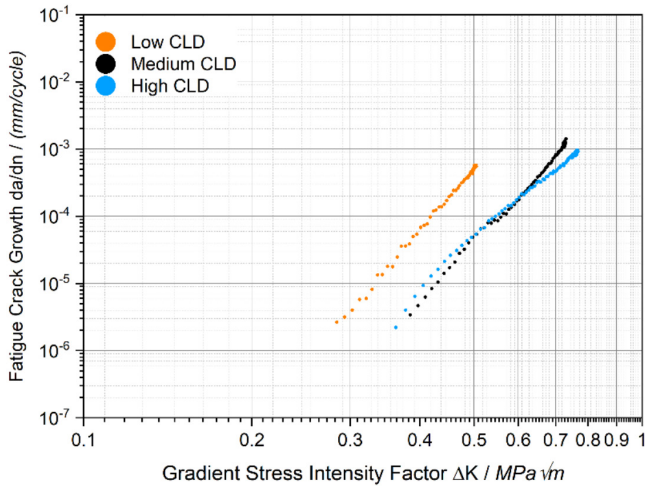

FIGURE 6 | Fatigue crack behavior of the three different resin systems. [Colour figure can be viewed at wileyonlinelibrary.com]

of tensile strength, the high cross-linked system outperforms the medium-CLD system, showing a 21% higher value. However, both systems exhibit similar elongation at break. In contrast to other systems, the low cross-linked system shows a lower tensile strength of 44.8 MPa, but a significantly higher elongation at break of 9.1%.

3.1.2 | Fatigue Properties

3.1.2.1 | Fatigue Crack Growth da/dn. The fatigue crack behavior of the resin systems is illustrated in Figure 6.

Regarding the onset of cracking, ΔK_{th}, the low cross-linked system exhibits an earlier detectable crack initiation at lower values of ΔK, compared to the medium and high cross-linked (CLD) systems. SEM images of the fracture surface at the crack onset, the medium cross-linked system displays a relatively smooth surface (Figure 7), the high cross-linked system, due to its cocontinuous morphology (as confirmed by AFM), exhibits a more ductile behavior with a "feather-like structure" and a rougher microsurface. In the Paris–Erdogan regime, both the medium and highly cross-linked systems exhibit shear bands, whereas the low cross-linked system shows a behavior similar to the onset stage.

In the high-stress regime, ΔK_{cf}, the high cross-linked sample exhibits a slight presence of feathering. The low-CLD sample still is similar to the onset stage. The reference sample displays a slight degree of roughness on the fracture surface, but still is similar to the other regimes. Based on these observations, we can conclude that in the high-CLD system there are three distinct regimes of crack behavior: (1) feathering at low stress, (2) cracking at moderate to high stress, and (3) reduced feathering at the highest stress levels. This variation is also evident in the slopes of the fatigue crack growth curves. In contrast, the low-CLD system demonstrates a consistent mechanism of crack propagation throughout the range of stress intensities. The fractography exhibits almost identical features, and the exponent ("slope") in the da/dN graph remains constant. The medium-CLD sample displays two (up to possibly three) regimes of crack growth, where the onset and end may follow the same mechanism, at least in terms of the slope. Similar fracture surface phenomena were recently reported for comparable PUR systems, where the resin composition was varied by mixing polymerized isocyanate MDI, polyether polyols and hydroxypropyl methacrylate (HPMA), leading to different moduli and strains at break. In

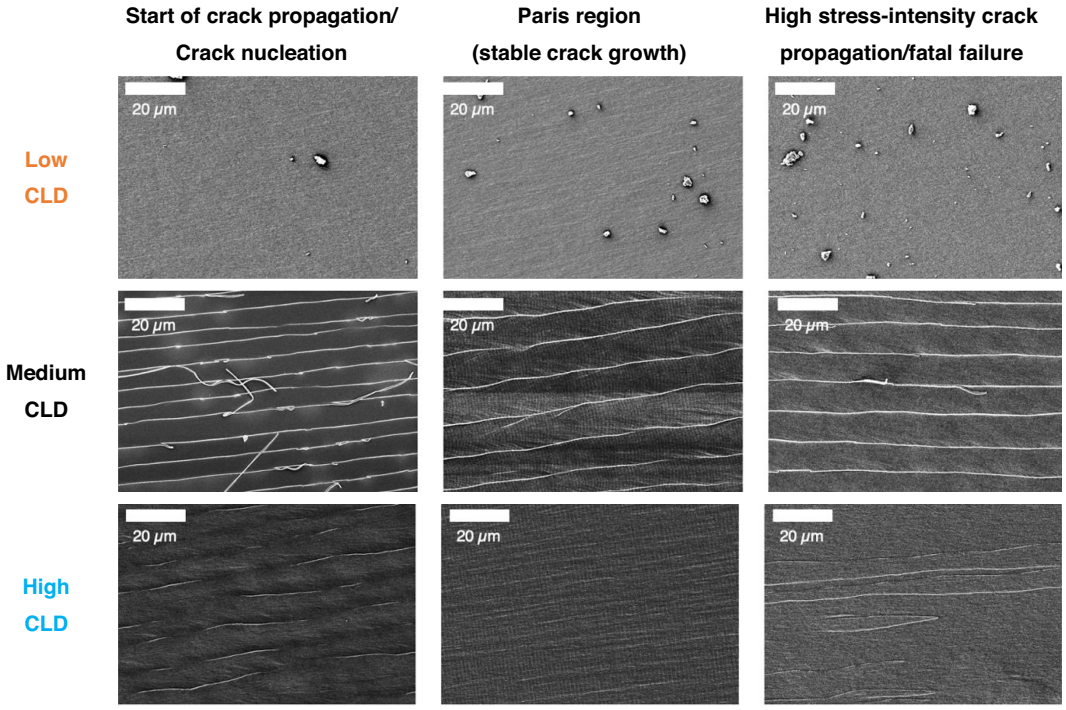

FIGURE 7 | SEM images of the fracture surfaces of the specific region of fatigue crack behavior. [Colour figure can be viewed at wileyonlinelibrary.com]

TABLE 3 | Properties of fatigue crack propagation of different resin systems.

Resin system	ΔKth MPa·m$^{0.5}$	ΔKcf MPa·m$^{0.5}$	m-slope (10^{-4} mm to 10^{-5} mm/cycle)
Low CLD	0.28	0.55	9.6
Medium CLD	0.32	0.73	9.3
High CLD	0.32	0.76	7.8

that study, similar to the present findings, a less refined yet more pronounced crack structure was observed with increasing stiffness, although neither the specific cross-link density nor the stress load of the analyzed fracture surface was reported [62].

Table 3 summarizes the characteristic values of all resin systems. The slope was determined in the region of stable crack growth between 10^{-4} and 10^{-5} mm/cycle. The high-CLD system exhibits the lowest slope in crack growth; however, it shows similar threshold (ΔK_{th}), and maximum (ΔK_{cf}) values compared to the medium-CLD system. This similarity is due to the presence of a "feathering mechanism" at low stress levels in the high-CLD system, which leads to a certain degree of energy absorption leading to lower slope and hence slightly slower stable crack growth compared to the medium-CLD system. On the other hand, the lowly cross-linked system maintains a consistent mechanism for crack propagation regardless of the stress level. It exhibits the highest slope and an earlier threshold value (ΔK_{th}) for crack initiation compared to the other systems.

3.1.2.2 | **Static Creep Tests.** Creep tests were performed for all three resin systems at different percentages of ultimate tensile strength (50%, 60%, and 70% of UTS), as shown in Figure 8. Results show that the highly cross-linked system exhibits the lowest creep strain at 50% and 60% loading compared to the other two systems. Furthermore, it demonstrates the ability to withstand the measurement duration of 500 h under both loadings. However, at 70% loading, the high-CLD system initially exhibits a high elastic strain of approximately 4%, which leads to failure at 6% strain after only 20 h, close to the quasi-static strain at break (5.4%).

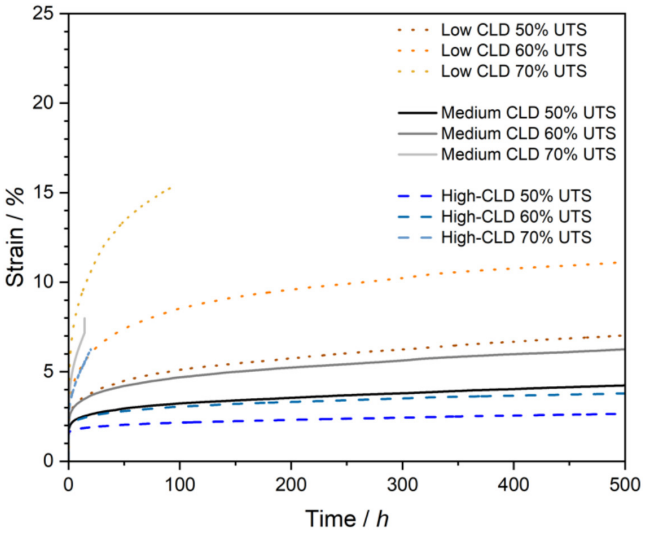

FIGURE 8 | Creep results of the resin systems at three different loadings. [Colour figure can be viewed at wileyonlinelibrary.com]

In contrast, the low-cross-linked system at 70% of UTS displays high strains of up to 15%, allowing for a longer creep time until

failure compared to the other systems (approximately 90 vs. 20 h). These strains significantly surpass the quasi-static strain at break of 9.3%. The loose network structure of the low-CLD system allows for higher strains before failure, as it does not restrict the reorientation of polymer chains as much as the medium- and high-CLD systems.

Therefore, the low-CLD system exhibits the ability to achieve higher strains before failure, indicating a greater capacity for polymer chain reorientation. Similar creep results were obtained with variation of stoichiometric ratio and different amine hardener and hence different cross-link density [63, 64].

3.1.2.3 | Residual Strength. Figure 9 shows the residual strength, where similar trends were observed for all three systems compared to the static creep tests. A minimal influence on tensile strength and a slight decrease in modulus were observed. The creep-loaded specimens exhibited a minor reduction in elongation at break of approximately 10%–14%. These findings demonstrate the high ductility of the PURs.

Similar observations were made by Koch et al. investigating ductile epoxy-based resin system after tensile creep measurements, where no decrease in properties was observed, and even higher strength and moduli were reported [22]. This was attributed to the orientation of epoxy polymer chains during creep, leading to a decrease in free volume and an increase in strength and stiffness.

In general, the three polyurethane systems with varying cross-link density show different behavior compared to epoxides, where higher CLD led to superior fatigue crack growth, better creep behavior, and residual strength. The high cross-link density and cocontinuous morphology lead to better mechanical properties. For the medium- and high-CLD systems, almost no deterioration of modulus and strength is observed. For low-CLD systems, the modulus slightly decreases, while residual strength after creep and strength of specimens with no creep loading are in the same range. As the strength shows no drastic decrease based on creep loading and this parameter would be highly affected by nucleated cracks, it is hypothesized that the fiber–matrix interaction and localized strain of the matrix is a decisive factor for the failure of the composites.

3.2 | Composite

To check the influence of fiber reinforcement on the mechanical properties especially with focus on fatigue properties, biaxial composites with ±45° glass noncrimped fabric (NCF) where produced. Due to the fiber setup, the matrix characteristics are strongly pronounced in the composite properties.

The fiber volume content, as determined via TGA measurements, was constant and at 59% for all produced composites.

3.2.1 | Static Mechanical Properties

Same tendencies in the composite for modulus and strength are visible compared to the neat resin systems with similar values for the medium-CLD and high-CLD system as can be seen in Table 4. For the interlaminar shear strength (ILSS), the low-CLD system showed the lowest values of 29 MPa, which can be attributed besides relatively inferior intrinsic matrix properties to rather poor bonding and weak adhesion between the fiber and the polyurethane matrix.

The strain at break of the composites relative to the neat resin reaches 76% for the neat low-CLD resin, 92% for medium CLD, and 100% for high CLD, which shows the best transfer of ductile behavior for the high-CLD resin. The opposite trend is observed for strength, where the low-CLD system profits the most from the glass fibers and the high-CLD system the least.

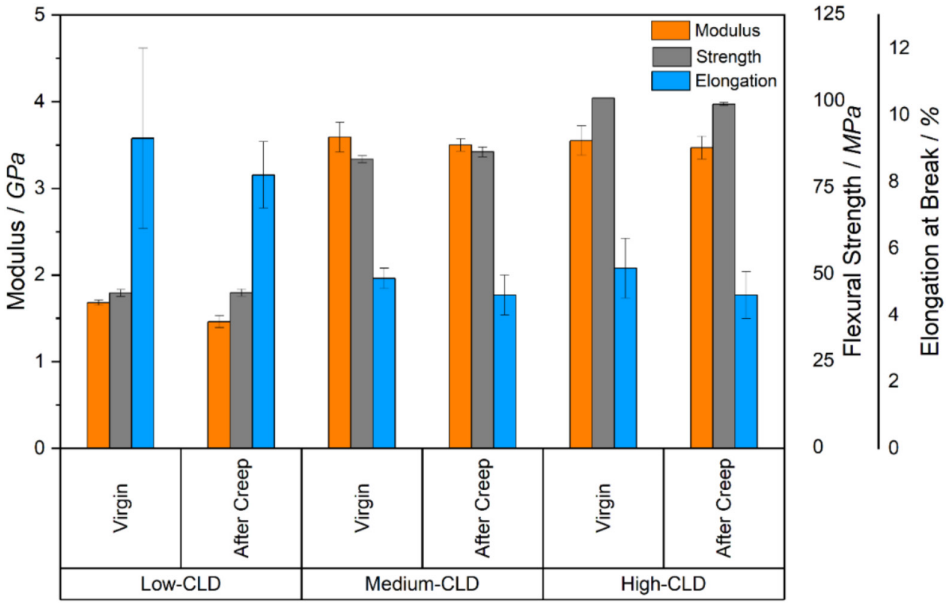

FIGURE 9 | Residual strength, modulus and elongation of the neat resin systems after creep loading of 50% of the ultimate strain at break loaded with 60% ultimate tensile stress. [Colour figure can be viewed at wileyonlinelibrary.com]

3.2.2 | SN Fatigue Tests

The results for tensile-tensile loading with $r = 0.1$ are shown as SN-curves in Figure 10.

The SN-curves depict the fatigue strength of the material under different stress levels. The dark-colored confidence bands represent the uncertainty of the power law fit and indicate the reliability of the obtained data/fit. Conversely, the bright-colored prediction band, which is also displayed, provides insights into the material's expected lifespan under specific loading conditions. To ensure the provision of statistically reliable design data, the analysis of the collected data involved selecting a scatter band associated with a 10% (upper limit) to 90% (lower limit) probability of survival.

Desirable fatigue performance is often related to delayed crack nucleation and slow crack growth. These characteristics are typically associated with high energy dissipation and plastic deformation occurring at the crack tip. The cross-link density of the resin matrix plays a role in balancing these characteristics to a certain extent.

TABLE 4 | Tensile properties, ILSS and T_g via DMA of the composite samples.

Properties	Low CLD	Medium CLD	High CLD
Tensile modulus/GPa	9.4±0.1	14.5±0.4	16.4±0.6
Tensile strength/MPa	102± 13	113± 5	126± 3
Strain at break/%	7.1± 0.3	4.7±0.7	5.4± 0.7
ILSS/MPa	29 ± 3	35 ± 3	42 ± 1
T_g onset/°C	68	77	85

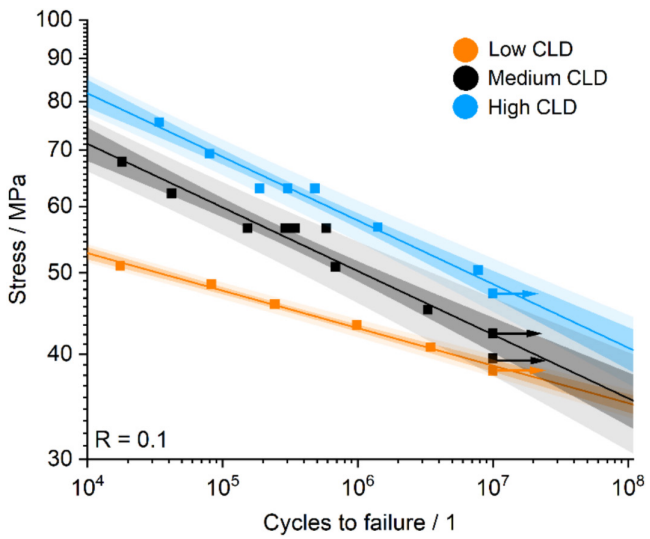

FIGURE 10 | SN curve of the three composite systems with a stress ratio $r = 0.1$ and frequency of 8 Hz. [Colour figure can be viewed at wileyonlinelibrary.com]

However, it is important to consider the potential drawbacks associated with extreme cross-link density variations. On the one hand, high cross-link densities can drive brittleness and reduce their impact resistance. On the other hand, low cross-link density can result in inadequate resistance to crack propagation and a diminished ability to evenly distribute stresses across the material, particularly in localized regions experiencing high-stress concentrations.

At relatively low-cycle numbers, around 10^4, in the "low cycle fatigue" region, the material experiences high stress level and rather plastic deformation. Here, the material with low cross-link density exhibits stress values approximately 25% lower than the reference sample and 36% lower compared to the material with high cross-link density. At the "high-cycle fatigue" region, with cycles around 10^7, the material experiences rather elastic deformation. Here, the stress values of the low-CLD system exhibit a reduction of only 10% compared to the medium-CLD sample, and a 25% decrease compared to the high-CLD system, approaching values closer to those of the other systems. This indicates that the low-CLD system demonstrates progressively improved performance at higher cycle numbers and lower loading. Surprisingly, this contradicts the initial assumption that the low-CLD system would perform better in the low-cycle fatigue region, where stronger ductile behavior was expected to prevail.

For the same applied load level, the material with high cross-link density shows a lifetime more than eight times longer, with a 90% probability of survival, compared to the medium-CLD sample. Furthermore, the slope of the stress–strain response curve for the high-CLD system matches that of the reference sample, albeit starting from about 20% higher initial load levels. The initial stress level is determined by the rate of crack nucleation, while the slope is influenced by plasticity and plays a role in comprehending the mechanism of crack propagation leading to better performance for the low-CLD system.

The slope of the SN fatigue test, or "k-factor," and the slope of the da/dN tests is shown in Table 5. For both the medium-CLD and high-CLD systems, the k-factor remains the same, mirroring the observations made in fatigue tests conducted with the neat resin, where the values displayed a high degree of alignment. In contrast, for the low-CLD system, the slope in the da/dN measurements had the highest slope, and therefore fast crack growth and potential earlier failure at the same stress intensity factor, whereas it shows in the SN fatigue test a high k-factor value with low slope and therefore lower load dependence on the fatigue life. This can be explained that the intrinsic brittle nature or relatively fast crack growth of the low-CLD resin seems to lead to

TABLE 5 | Material fatigue performance of neat resin and GFRP composite indicated by slope of measurement data.

Resin system	Slope composite k-factor	Slope neat resin da/dN
Low CLD	22.4	9.5
Medium CLD	13.2	7.0
High CLD	13.2	8.1

homogenously distributed microcracks and less load influence on the fatigue lifetime.

Furthermore, fiber–matrix adhesion of the different resin systems might partially explain the difference in quasi-static and fatigue properties although the resins share similar chemical nature.

However, in absolute values, the low CLD shows a lower fatigue life at any given stress compared to medium and high CLD up to 10^7 cycles. This behavior may be attributed to the low modulus and low strength of the ductile matrix. As discussed, the high elongation at break of the matrix is only reflected to a small extent in the composite. Furthermore, the low-CLD system showed rather brittle behavior in fatigue crack growth tests.

To gain a deeper material understanding, the degradation in stiffness was evaluated by measuring the decrease in dynamic modulus during fatigue loading at specific load levels (37.5%, 45%, and 50% of the ultimate tensile strength, see Figure 11). The dynamic modulus was determined by analyzing the stress and strain data obtained from the hysteresis curves, based on the piston path. In the case of all stress levels, the material with low cross-link density initially exhibited a significantly lower modulus, which can be attributed to matrix cracking, as already indicated by the crack growth rate (da/dN).

At a stress level of 37.5%, none of the three systems experienced catastrophic failure and they remained structurally intact. For the higher loadings, the characteristic S-shape with first initial reduction in modulus, a plateau region, and subsequent fatal failure is observed.

In the second phase of the fatigue process, cracks exhibit steady growth. Thus, the modulus of the material decreases linearly. Subsequently, during the third phase, microcracks interconnect and evolve into macro cracks, resulting in a significant loss of modulus and accelerated strain development. This deformation pattern leads to the occurrence of fatigue failure in the material.

Similarly, when considering the material's capacity to withstand the applied load in the SN diagram, the difference in the change of modulus between the systems becomes more pronounced, particularly at higher loads with the low-CLD system. Despite the higher elongation at break and the consequent ability of the neat resin system to withstand higher strain levels, the subsequent decrease in modulus does not translate into an extended lifetime of the composite.

4 | Summary and Outlook

Achieving an optimal balance between stiffness, strength and toughness is essential for composite performance and fatigue lifetime. In this context, resin cross-link density is often cited as a crucial factor influencing fatigue properties. In this study, the crack initiation and growth in neat PUR resins with different cross-link densities and the tensile fatigue performance of their corresponding glass fiber-reinforced polymer composites were investigated. Three PUR systems with different cross-link densities were formulated and the characterization of both neat resin and glass–fiber composites revealed the thermomechanical properties, morphology, creep resistance, and fatigue behavior. DMA was used to determine the thermomechanical profile, storage modulus, glass transition temperatures (T_g), and hence cross-link densities of the PUR resin systems. The low-CLD and high-CLD system exhibited a bimodal tan(δ) and a significant shoulder in the T_g region, indicating the presence of a second phase. Atomic force microscopy (AFM) confirmed the phase separation and revealed different morphologies in the three resin systems.

Fatigue crack growth measurements of the neat resin and SEM images of the fracture surface provided insights into the crack resistance and ductility of the resin systems. The low-CLD system exhibited earlier crack initiation and more brittle behavior, while the high-CLD system showed a feathering mechanism leading to slower crack growth. Residual strength analysis was performed on the neat resin systems to examine the impact of long-term strain (average medium stress) and estimate damage evolution during cyclic fatigue testing in the matrix of composites. Only minimal influence of precreep on tensile strength, a slight decrease in modulus, and a small reduction in elongation at break was determined for all three resin systems. This proves that in interplay with the fiber reinforcement pronounced crack initiation and crack growth take place.

Fatigue tests of the composites revealed a shorter fatigue life of the low-CLD system compared to the medium- and high-CLD systems, possibly due to its low modulus and fracture toughness. The dynamic modulus decreased during fatigue loading,

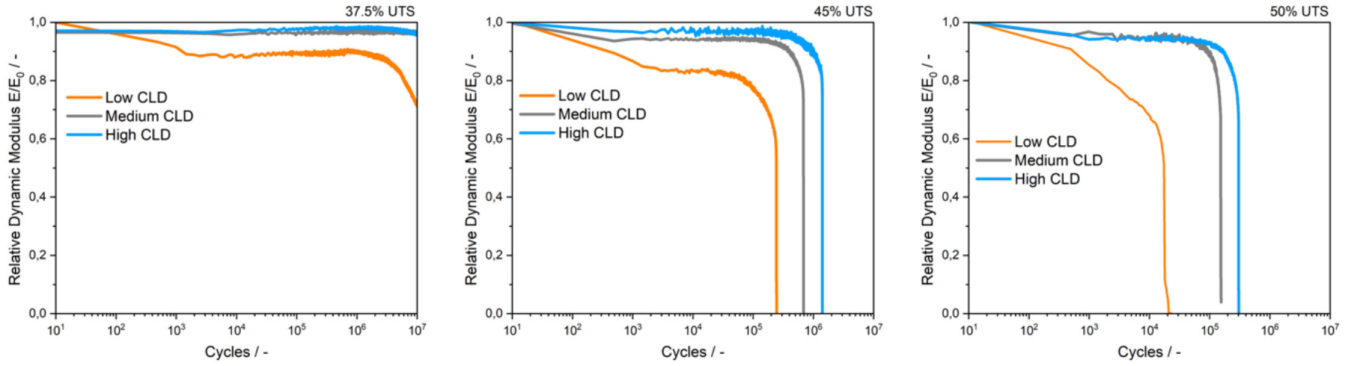

FIGURE 11 | Dynamic modulus development of the resin systems at different loading conditions. [Colour figure can be viewed at wileyonlinelibrary.com]

indicating the occurrence of matrix cracking and subsequent failure. The difference in modulus loss between systems became more pronounced at higher loads, highlighting the impact of cross-link density on fatigue performance. Here, the residual stiffness drop is lower for laminates with stronger resin matrix showing that high cross-link density and strength is relevant for high loadings. As shown in the residual strength experiments, the interaction between fiber and matrix is a promising future topic to be studied (e.g., by fiber pull-/pushout) as this property is likely a significant factor and could also superimpose the effect of CLD (and morphology) on the composite fatigue properties. Furthermore, it is hypothesized that also the morphology of the high-CLD system compared to the medium-CLD system is another reason for its superior performance. This is due to the morphology consisting of a more brittle continuous phase with droplets with higher ductility. Similar mechanisms are known in epoxy resins leading to better mechanical properties [65–67].

In conclusion, this study emphasizes the critical importance of achieving an optimal balance between stiffness and strength with toughness in composite materials, specifically focusing on the impact of resin cross-link density and resin morphology on resin fatigue properties and the resulting performance of glass fiber-reinforced polymer composites in quasi-static and fatigue loading. The findings suggest that cross-link density alone cannot fully predict fatigue behavior, and future research should further explore interfacial mechanics and phase morphology to develop fatigue-optimized composite materials. However, this work lays a foundation for the targeted design of resin systems in high-performance composites, paving the way for improved durability and reliability in fatigue-critical applications.

Author Contributions

Martin Demleitner: conceptualization, formal analysis, investigation, writing – original draft. **Daniel Raps:** conceptualization, formal analysis, writing – original draft. **Sarah Mäker:** investigation, review and editing. **Qi Chen:** investigation, review and editing. **Alexander Brückner:** investigation, review and editing. **Holger Ruckdäschel:** conceptualization, review and editing, project administration.

Acknowledgements

Open Access funding enabled and organized by Projekt DEAL.

Data Availability Statement

The data that support the findings of this study are available from the corresponding author upon reasonable request.

References

1. H. Yousefi, A. Abbaspour, and H. Seraj, "Worldwide Development of Wind Energy and CO2 Emission Reduction," *Environmental Energy and Economic Research* 3 (2019): 1–9, https://doi.org/10.22097/eeer.2019.164295.1064.

2. R. A. Zakhidov, "Modern Trends in Wind-Power Engineering," *Applied Solar Energy* 44 (2008): 147–148, https://doi.org/10.3103/S0003701X08020217.

3. Wind Turbine Blades—The Global Market 2020, "AMI Report," (2020).

4. N. Vahedi, C. Wu, A. P. Vassilopoulos, and T. Keller, "Thermomechanical Characterization of a Balsa-Wood-Veneer Structural Sandwich Core Material at Elevated Temperatures," *Construction and Building Materials* 230 (2020): 117037, https://doi.org/10.1016/J.CONBUILDMAT.2019.117037.

5. M. Borrega and L. J. Gibson, "Mechanics of Balsa (*Ochroma pyramidale*) Wood," *Mechanics of Materials* 84 (2015): 75–90, https://doi.org/10.1016/J.MECHMAT.2015.01.014.

6. G. Newaz, M. Mayeed, and A. Rasul, "Characterization of Balsa Wood Mechanical Properties Required for Continuum Damage Mechanics Analysis," *Proceedings of the Institution of Mechanical Engineers, Part L, Journal of Materials Design and Applications* 230 (2016): 206–218, https://doi.org/10.1177/1464420714564711/ASSET/IMAGES/LARGE/10.1177_1464420714564711-TABLE3.JPEG.

7. J. A. da Cruz, E. F. Kerche, O. Bianchi, et al., "Castor Oil-Based Polyurethane/S2 Glass/Aramid Hybrid Composites Manufactured by Vacuum Infusion," *Polymer* 14 (2022): 5150, https://doi.org/10.3390/POLYM14235150.

8. J. Maas, D. Soontjens, E. Mojica Silva, et al., "Leveraging Advanced Polyurethane Resins and Coatings to Develop High-Performance Wind Turbine Blades," (2022).

9. P. A. Filis, I. R. Farrow, and I. P. Bond, "Classical Fatigue Analysis and Load Cycle Mix-Event Damage Accumulation in Fibre Reinforced Laminates," *International Journal of Fatigue* 26 (2004): 565–573, https://doi.org/10.1016/j.ijfatigue.2003.10.013.

10. V. Altstädt, "Effect of the Polymer Matrix on the Properties of Advanced Composites," in *Makromolekulare Chemie. Macromolecular Symposia* (Hüthig & Wepf Verlag, 1991), https://doi.org/10.1002/masy.19910500114.

11. M. F. Horstemeyer and G. H. Staab, "Interface Debonding in Fatigue Cycling of Glass Reinforced Plastics," *Journal of Reinforced Plastics and Composites* 9 (1990): 446–455, https://doi.org/10.1177/073168449000900502.

12. J. Gassan and T. Dietz, "Fatigue Behavior of Cross-Ply Glass-Fiber Composites Based on Epoxy Resins of Different Toughnesses," *Composites Science and Technology* 61 (2001): 157–163, https://doi.org/10.1016/S0266-3538(00)00205-0.

13. C. M. Manjunatha, S. Sprenger, A. C. Taylor, and A. J. Kinloch, "The Tensile Fatigue Behavior of a Glass-Fiber Reinforced Plastic Composite Using a Hybrid-Toughened Epoxy Matrix," *Journal of Composite Materials* 44 (2010): 2095–2109, https://doi.org/10.1177/0021998309360943.

14. M. H. R. Jen, Y. S. Kau, and C. L. Ong, "Effect of Matrix Resin on the Response in a Centrally Notched Composite Laminate," *Composite Structures* 29 (1994): 99–106, https://doi.org/10.1016/0263-8223(94)90039-6.

15. S. K. Joneja, "Matrix Contribution to Fatigue Behavior of Glass Reinforced Polyester Composites," *Journal of Reinforced Plastics and Composites* 6 (1987): 343–356, https://doi.org/10.1177/073168448700600404.

16. A. Müller, "Schädigungscharakterisierung an Faser-Kunststoff-Verbunden im Schwingversuch mittels Röntgenrefraktionstopographie unter Berücksichtigung der Matrixeigenschaften," 2018.

17. M. R. Loos, J. Yang, D. L. Feke, and I. Manas-Zloczower, "Enhanced Fatigue Life of Carbon Nanotube-Reinforced Epoxy Composites," *Polymer Engineering and Science* 52 (2012): 1882–1887, https://doi.org/10.1002/pen.23145.

18. G. C. Jacob, B. Hoevel, and H. Q. Pham, "Technical Advances in Epoxy Technology for Wind Turbine Blade Composite Fabrication, in: Int. SAMPE Tech. Conf," (2009).

19. M. A. Mousavi Khorasani, S. Sahebian, and A. Zabett, "Effects of Toughened Polyester on Fatigue Behavior of Glass Fiber Reinforced Polyester Composite for Wind Turbine Blade," *Polymer Composites* 42 (2021): 70–82, https://doi.org/10.1002/pc.25808.

20. E. K. Gamstedt and R. Talreja, "Fatigue Damage Mechanisms in Unidirectional Carbon-Fibre-Reinforced Plastics," *Journal of Materials Science* 34 (1999): 2535–2546, https://doi.org/10.1023/A:1004684228765.

21. C. Henaff-Gardin and M. C. Lafarie-Frenot, "Fatigue Behaviour of Thermoset and Thermoplastic Cross-Ply Laminates," *Composites* 23 (1992): 109–116, https://doi.org/10.1016/0010-4361(92)90111-7.

22. I. Koch, G. Just, M. Brod, et al., "Evaluation and Modeling of the Fatigue Damage Behavior of Polymer Composites at Reversed Cyclic Loading," *Materials (Basel)* 12 (2019): 1727–1749, https://doi.org/10.3390/ma12111727.

23. M. Demleitner, F. Schönl, J. Angermann, et al., "Influence of Block Copolymer Concentration and Resin Crosslink Density on the Properties of UV-Curable Methacrylate Resin Systems," *Macromolecular Materials and Engineering* 307 (2022): 2200320, https://doi.org/10.1002/MAME.202200320.

24. F. Hübner, E. Szpoganicz, M. Demleitner, J. Kuhnigk, V. Altstädt, and A. de Rios Anda, "Time Domain 1 H NMR, Thermomechanical, and Rheology Multiscale Structural Characterization of Polydimethylsiloxane-Toughened Epoxy Nanocomposites for Liquid Composite Molding," *ACS Applied Polymer Materials* 2 (2020): 4779–4789, https://doi.org/10.1021/acsapm.0c00763.

25. J. D. Hübsch, M. Demleitner, S. Bard, et al., "Influence of Skydrol Immersion at Elevated Temperatures on the Thermo-Mechanical Properties of a High-Tg Anhydride Epoxy Resin Toughened With a Hydroxy-Terminated Polyester," *Journal of Applied Polymer Science* 140 (2023): e53263, https://doi.org/10.1002/APP.53263.

26. F. S. Sorce, T. Shields, S. Ngo, C. Lowe, and A. C. Taylor, "The Effect of Varying Molecular Weight on the Performance of HMMM-Crosslinked Polyester Coatings," *Progress in Organic Coatings* 149 (2020): 105920, https://doi.org/10.1016/j.porgcoat.2020.105920.

27. S. Katoch and P. P. Kundu, "Thermal and Mechanical Behavior of Unsaturated Polyester [Derived From Poly (Ethylene Terephthalate) Waste] and Montmorillonite-Filled Nanocomposites Synthesized by In Situ Polymerization," *Journal of Applied Polymer Science* 122 (2011): 2731–2740, https://doi.org/10.1002/app.34042.

28. N. T. Qazvini and N. Mohammadi, "Dynamic Mechanical Analysis of Segmental Relaxation in Unsaturated Polyester Resin Networks: Effect of Styrene Content," *Polymer* 46 (2005): 9088–9096, https://doi.org/10.1016/j.polymer.2005.06.118.

29. M. Kubouchi, H. Sembokuya, N. Takahashi, and K. Tsuda, "Corrosion Behavior of Unsaturated Polyester Resins With Different Crosslink Density," *Zairyo-to-Kankyo* 53 (2004): 258–263, https://doi.org/10.3323/jcorr1991.53.258.

30. C. Liu, W. Lei, Z. Cai, et al., "Use of Tung Oil as a Reactive Toughening Agent in Dicyclopentadiene-Terminated Unsaturated Polyester Resins," *Industrial Crops and Products* 49 (2013): 412–418, https://doi.org/10.1016/j.indcrop.2013.05.023.

31. Q. Zou, F. Xiao, S. Q. Gu, et al., "Toughening of Bismaleimide Resin Based on the Self-Assembly of Flexible Aliphatic Side Chains," *Industrial and Engineering Chemistry Research* 58 (2019): 16526–16531, https://doi.org/10.1021/acs.iecr.9b01822.

32. J. Hu, A. Gu, G. Liang, D. Zhuo, and L. Yuan, "Preparation and Properties of Mesoporous Silica/Bismaleimide/Diallylbisphenol Composites With Improved Thermal Stability, Mechanical and Dielectric Properties," *Express Polymer Letters* 5 (2011): 555–568, https://doi.org/10.3144/expresspolymlett.2011.54.

33. 学. 宇志小林, 俊. 大山, 俊. 大山, et al., "エポキシ変性速硬化性シアナートエステル樹脂の研究," ネットワークポリマー 33 (2012): 130–139, https://doi.org/10.11364/NETWORKPOLYMER.33.130.

34. O. Georjon and J. Galy, "Effects of Crosslink Density on the Volumetric Properties of High Tg Polycyanurate Networks. Consequences on Moisture Absorption," *Polymer* 39 (1998): 339–345, https://doi.org/10.1016/S0032-3861(97)00267-X.

35. J. Li, C. Ren, D. An, Y. Ren, K. Moon, and C. Wong, "Systematic Evaluation of Cyanate Ester/Epoxidized Cresol Novolac Copolymer Resin System for High Temperature Power Electronic Packaging Applications," *Polymer* 195 (2020): 122454, https://doi.org/10.1016/J.POLYMER.2020.122454.

36. H. Yan, T. Li, M. Zhang, et al., "Mechanical and Dielectric Properties of Blends of Dicyanate Ester and Bisphenol A-Based Benzoxazine," *High Performance Polymers* 26 (2014): 618–624, https://doi.org/10.1177/0954008314526423.

37. Y. Wang, K. Kou, G. Wu, L. Zhuo, J. Li, and Y. Zhang, "The Curing Reaction of Benzoxazine With Bismaleimide/Cyanate Ester Resin and the Properties of the Terpolymer," *Polymer* 77 (2015): 354–360, https://doi.org/10.1016/J.POLYMER.2015.09.059.

38. G. Wu, Y. Cheng, Q. Xie, et al., "Synthesis of a Bismaleimide/Cyanate Ester Copolymer Containing Phenolphthalein Functional Group With Excellent Dielectric Properties and Thermally Stable," *Journal of Polymer Research* 21, no. 12 (2014): 1–8, https://doi.org/10.1007/S10965-014-0615-0.

39. Y. Ohnishi, T. Oyama, and A. Takahashi, "多環芳香族型エポキシ樹脂の硬化性と熱機械特性," 高分子論文集 68 (2011): 62–71, https://doi.org/10.1295/KORON.68.62.

40. W. Liu, Q. Qiu, J. Wang, Z. Huo, H. Sun, and X. Zhao, "Preparation and Properties of One Epoxy System Bearing Fluorene Moieties," *Journal of Applied Polymer Science* 113 (2009): 1289–1297, https://doi.org/10.1002/APP.30141.

41. I. Ogura and Y. Takahashi, "Multi-Functional Epoxy Resins Performing High Thermal Resistance With Good Flow-Ability Based on Dimeric Naphthols," *High Performance Polymers* 22 (2010): 834–847, https://doi.org/10.1177/0954008309347638.

42. V. Bellenger, J. Verdu, and E. Morel, "Structure-Properties Relationships for Densely Cross-Linked Epoxide-Amine Systems Based on Epoxide or Amine Mixtures—Part 2 Water Absorption and Diffusion," *Journal of Materials Science* 24 (1989): 63–68, https://doi.org/10.1007/BF00660933/METRICS.

43. S. Grishchuk, S. Schmitt, O. C. Vorster, et al., "Structure and Properties of Amine-Hardened Epoxy/Benzoxazine Hybrids: Effect of Epoxy Resin Functionality," *Journal of Applied Polymer Science* 124 (2012): 2824–2837, https://doi.org/10.1002/APP.35302.

44. J. A. Schroeder, P. A. Madsen, and R. T. Foister, "Structure/Property Relationships for a Series of Crosslinked Aromatic/Aliphatic Epoxy Mixtures," *Polymer* 28 (1987): 929–940, https://doi.org/10.1016/0032-3861(87)90165-0.

45. H. A. Federolf, P. Eyerer, B. Möginger, C. Mebus, R. Jin, and W. Scheer, "Study on Epoxy Novolac and Carbon-Fiber Reinforced Epoxy Novolac Composites for Use as Implant Materials. Part 1. Mechanical and Viscoelastic Properties," *Journal of Polymer Engineering* 19 (1999): 243–264, https://doi.org/10.1515/POLYENG.1999.19.4.243/MACHINEREADABLECITATION/RIS.

46. E. Espuche, J. Galy, J.-F. Gérard, et al., "Influence of Crosslink Density and Chain Flexibility on Mechanical Properties of Model Epoxy Networks," *Macromolecular Symposia* 93 (1995): 107–115, https://doi.org/10.1002/MASY.19950930115.

47. N. Rasoldier, X. Colin, J. Verdu, et al., "Model Systems for Thermo-Oxidised Epoxy Composite Matrices," *Composites Part A, Applied Science and Manufacturing* 39 (2008): 1522–1529, https://doi.org/10.1016/J.COMPOSITESA.2008.05.016.

48. J. D. Tanks, M. Kubouchi, and Y. Arao, "Influence of Network Structure on the Degradation of Poly (Ether)amine-Cured Epoxy Resins by Inorganic Acid," *Polymer Degradation and Stability* 157 (2018): 153–159, https://doi.org/10.1016/J.POLYMDEGRADSTAB.2018.10.011.

49. Y. Qi, J. Wang, Y. Kou, et al., "Synthesis of an Aromatic N-Heterocycle Derived From Biomass and Its Use as a Polymer Feedstock," *Nature Communications* 10, no. 1 (2019): 1–9, https://doi.org/10.1038/s41467-019-10178-0.

50. "DNVGL-ST-0376 Rotor Blades for Wind Turbines," (2015).

51. M. Kempf, S. Schwägele, A. Ferencz, et al., "ICCM Int. Conf. Compos. Mater," (2011).

52. S. Gloggnitzer, T. Buchsteiner, and G. Pilz, "Influence of the Manufacturing Parameters on Mechanical Properties of Polyurethane Based Composites, in: 16th Eur. Conf. Compos. Mater. ECCM 2014," (2014).

53. D. Huelsbusch, M. Jamrozy, S. Mrzljak, et al., "Mechanism-Oriented Characterization of the Fatigue Behavior of Glass Fiber-Reinforced Polyurethane Based on Hysteresis and Temperature Measurements," *Key Engineering Materials* 742 (2017): 629–635, https://doi.org/10.4028/www.scientific.net/KEM.742.629.

54. D. Hülsbusch, R. Helwing, S. Mrzljak, et al., "Comparison of the Damage Evolution in Glass Fiber-Reinforced Polyurethane and Epoxy in the HCF and VHCF Regimes Investigated by Intermittent In Situ X-Ray Computed Tomography," in *IOP Conference Series: Materials Science and Engineering* (IOP Publishing. 2020), https://doi.org/10.1088/1757-899X/942/1/012036.

55. W. Han, P. Zhou, S. Xie, C. Li, G. Xian, and S. Dong, "A Review of the Mechanical Property, Durability, and Modification of Carbon- and Glass-Fiber Reinforced Polyurethane Composites," *Polymer Composites* 46 (2025): 7819–7837.

56. Y. Li, S. Peng, J. T. Miao, et al., "Isotropic Stereolithography Resin Toughened by Core-Shell Particles," *Chemical Engineering Journal* 394 (2020): 124873, https://doi.org/10.1016/j.cej.2020.124873.

57. S. Bard, M. Demleitner, R. Weber, R. Zeiler, and V. Altstädt, "Effect of Curing Agent on the Compressive Behavior at Elevated Test Temperature of Carbon Fiber-Reinforced Epoxy Composites," *Polymers (Basel)*. 11 (2019): 943, https://doi.org/10.3390/polym11060943.

58. M. H. Kothmann, R. Zeiler, A. Rios De Anda, A. Brückner, and V. Altstädt, "Fatigue Crack Propagation Behaviour of Epoxy Resins Modified With Silica-Nanoparticles," *Polymer* 60 (2015): 157–163, https://doi.org/10.1016/j.polymer.2015.01.036.

59. M. H. Kothmann, G. Bakis, and R. Zeiler, "Influence of Nanoparticles on the Fatigue Crack Growth Behavior of Epoxy Resins, in: 16th Eur. Conf. Compos. Mater. ECCM 2014," (2014).

60. S. Dadbin, R. P. Burford, and R. P. Chaplin, "Interpenetrating Polymer Networks of Poly (Allyl Diglycol Carbonate) and Polyurethane: Effect of Composition and Crosslink Density on Morphology and Mechanical Properties," *Polymer* 37 (1996): 785–792, https://doi.org/10.1016/0032-3861(96)87254-5.

61. D. S. Le and S. C. Kim, "Polyurethane Interpenetrating Polymer Networks (IPN'S) Synthesized Under High Pressure. 2. Morphology and Tg Behavior of Polyurethane-Polystyrene IPN'S," *Macromolecules* 17 (1984): 2193–2196, https://doi.org/10.1021/MA00140A053.

62. Z. Jiang, L. Li, L. Fu, G. Xiong, H. Wu, and S. Guo, "Efficient Regulation of the Cross-Linking Structure in Polyurethane: Achieving Outstanding Processing and Mechanical Properties for a Wind Turbine Blade," *Polymers (Basel)* 16 (2024): 235, https://doi.org/10.3390/polym16020235.

63. N. Mattar, F. Hübner, M. Demleitner, et al., "Multiscale Characterization of Creep and Fatigue Crack Propagation Resistance of Fully Bio-Based Epoxy-Amine Resins," *ACS Applied Polymer Materials* 3 (2021): 5134–5144, https://doi.org/10.1021/acsapm.1c00894.

64. M. Demleitner, F. Hübner, A. Mainz, et al., "Influence of Network Structure Determined by Time-Domain ^{1}H Double Quantum NMR on the Creep Properties of Non-Stoichiometric Epoxy-Amine Resins Aimed for Chemical Anchoring Applications," *Polymer* 286 (2023): 126373, https://doi.org/10.1016/J.POLYMER.2023.126373.

65. K. A. Masser, E. D. Bain, F. L. Beyer, A. M. Savage, J. H. Yu, and J. L. Lenhart, "Influence of Nano-Scale Morphology on Impact Toughness of Epoxy Blends," *Polymer* 103 (2016): 337–346, https://doi.org/10.1016/J.POLYMER.2016.09.076.

66. R. Akbari, M. H. Beheshty, and M. Shervin, "Toughening of Dicyandiamide-Cured DGEBA-Based Epoxy Resins by CTBN Liquid Rubber," *Iranian Polymer Journal* 22 (2013): 313–324, https://doi.org/10.1007/S13726-013-0130-X/FIGURES/12.

67. L. L. Sobrinho, V. M. A. Calado, and F. L. Bastian, "Effects of Rubber Addition to an Epoxy Resin and Its Fiber Glass-Reinforced Composite," *Polymer Composites* 33 (2012): 295–305, https://doi.org/10.1002/PC.21265.

Supporting Information

Additional supporting information can be found online in the Supporting Information section. **Data S1:** Supporting information.